Chaos, Solitons and Fractals 180 (2024) 114497

Contents lists available at ScienceDirect

Chaos, Solitons and Fractals

journal homepage: www.elsevier.com/locate/chaos

Peakons in spinor $F = 1$ Bose–Einstein condensates with $\mathcal{PT}$-symmetric δ-function potentials

Jun-Yi Lao, Zi-Yang Qin, Jia-Rui Zhang, Yu-Jia Shen *

College of Science, China Agricultural University, Beijing 100083, China

ARTICLE INFO

Keywords:
Peakons
Spinor $F = 1$ Bose–Einstein condensates
$\mathcal{PT}$-symmetric δ-function potentials

ABSTRACT

By introducing $\mathcal{PT}$-symmetric δ-function potentials into three-component Gross–Pitaevskii equations that describe spinor $F = 1$ Bose–Einstein condensates, we obtain stable and unstable analytical peakon solutions which enable us to explore the patterns of mean-field and spin-exchange interaction in relation to variations in energy of nonlinear modes. Furthermore, using iterative algorithms, we generate a series of numerical solutions and represent several families of peakon solutions in the form of energy curves, examining the impact of parameters on energy. Additionally, we observe a closed-loop structure in the family of peakons, with P_0 and μ_0 serving as the coordinate axes. On this curve, we discover stable peakons exhibiting periodic oscillatory properties, which can be regarded as a form of internal energy transfer within the coupled system. This research could contribute to a more comprehensive understanding of coupled nonlinear systems and serve as a reference for future experiments in this domain.

1. Introduction

Bose–Einstein condensates (BECs), the phenomenon of a pronounced increase in wave-like behavior as temperature decreases in atomic gases, has enabled the expansion of quantum mechanics into macroscopic sizes [1]. Recent years have witnessed diverse research fields concerning BECs [2–5], a single-component $\mathcal{PT}$-symmetric Gross–Pitaevskii equation (GPE) describing a fundamental category of the systems has also been extensively studied [6–10]. As an intriguing field within condensed matter physics, these studies have delved into topics such as liquid quantum droplets, dipolar supersolids [11,12], and simulating superfluid-to-Mott insulator transition in twisted-bilayer square lattices [13]. In various studies on BECs, the introduction of spin particles has emerged as a focal point, particularly with the significant development of spintronics and quantum information science. A more complex and realistic dynamic system is described by spin-F BECs, which differs from standard BECs by taking into account the interaction between particle spin and orbital motion [14–17]. This model offers new possibilities for the development and application of quantum information processing, quantum simulation, and quantum computing technologies. A growing number of relevant experiments, such as Raman lasers induced transitions [18–20], spin currents induced by spin-dependent force [21,22], and vortex-lattice formation [23,24], are further driving the need for the refinement of associated theories.

On the other hand, the δ-function describing quantities in limiting cases finds extensive applications in nonlinear systems in quantum mechanics. For example, it is used in the study of collective excitations of one-dimensional quantum droplets [25–27], the research of self-adjoint extensions in the propagation of quantum fields for Dirac operators [28], as well as the analysis of fast soliton scattering [29]. Previous interesting studies pointed out that $\mathcal{PT}$-symmetry can make non-Hermitian Hamiltonian systems with complex-valued potentials possibly support fully real linear spectra and stable nonlinear modes [6,30]. Moreover, $\mathcal{PT}$-symmetric δ-function potentials support stable peakons in the Kerr nonlinear Schrödinger equation (NLSE) [31,32]. The NLSE involving the introduction of δ-function potentials has been explored in depth, enhancing our comprehension of the description of a planar waveguide in nonlinear optics [33–36]. Similarly, focusing on the study of peakons is particularly advantageous as it allows for a deeper understanding of the introduction of δ-function potentials in BECs, local perturbations, defects, and interactions in nonlinear systems. Thus, some research has analyzed one-dimensional/quasi-one-dimensional spin-0 BECs systems, including the exact peakon solutions in the Salerno model [37,38], the drag force on an impurity in the superfluidity of quasi-one-dimensional BECs [39,40], and the introduction of $\mathcal{PT}$-symmetric double-δ potentials in the GPE [41–43]. However, there has been relatively little research on peakons in multi-component nonlinear systems with a spinor order parameter $F = 1$.

In this paper, based on above reasons, we introduce $\mathcal{PT}$-symmetric δ-function potential into the spin-1 BECs, described by a system of

* Corresponding author.
E-mail address: yjshen2018@cau.edu.cn (Y.-J. Shen).

https://doi.org/10.1016/j.chaos.2024.114497
Received 8 November 2023; Received in revised form 17 January 2024; Accepted 17 January 2024

three coupled GPEs. The corresponding generalized Hamiltonian of the mean-field spin-1 BECs system can be written as

$$H=\int\left\{\left[\boldsymbol{\Psi}^{\dagger}(\frac{\hbar^2}{2m}\partial_x^2+\boldsymbol{V})\boldsymbol{\Psi}\right]+\left[\frac{1}{2}c_0n^2+\frac{1}{2}c_2|\boldsymbol{F}|^2\right]\right\}dx, \tag{1}$$

where $\boldsymbol{\Psi}(x,t)=(\psi_+,\psi_0,\psi_-)^{\mathrm{T}}$ is a vector order parameter, "†" denotes the matrix conjugate transpose, $\hbar$ is the reduced Planck constant, m denotes the atomic mass, i denotes the imaginary unit, $n=|\psi_+|^2+|\psi_0|^2+|\psi_-|^2$ is the particle density, $\boldsymbol{F}=(F_x,F_y,F_z)^{\mathrm{T}}$ is the spin polarization vector with $F_\mu=\boldsymbol{\Psi}^{\dagger}\hat{f}_\mu\boldsymbol{\Psi}$ ($\mu=x,y,z$), c_0 and c_2 represent the mean-field and spin-exchange interaction, respectively [44,45]. In this case, the external potential matrix and the spin matrices are defined as

$$\boldsymbol{V}=\begin{bmatrix}V_+(x)&0&0\\0&V_0(x)&0\\0&0&V_-(x)\end{bmatrix},\quad \hat{f}_x=\frac{1}{\sqrt{2}}\begin{bmatrix}0&1&0\\1&0&1\\0&1&0\end{bmatrix},$$
$$\hat{f}_y=\frac{\mathrm{i}}{\sqrt{2}}\begin{bmatrix}0&-1&0\\1&0&-1\\0&1&0\end{bmatrix},\quad \hat{f}_z=\begin{bmatrix}1&0&0\\0&0&0\\0&0&-1\end{bmatrix}.$$

Governed by the variational principle $\mathrm{i}\hbar\partial_t\psi_j=\delta H/\delta\psi_j^*$ ($j=+,0,-$), the corresponding GPEs can be expressed as

$$\begin{aligned}
\mathrm{i}\hbar\partial_t\psi_+=&-\frac{\hbar^2}{2m}\partial_x^2\psi_++V_+(x)\psi_++(c_0+c_2)(|\psi_+|^2+|\psi_0|^2)\psi_+\\
&+(c_0-c_2)|\psi_-|^2\psi_++c_2\psi_0^2\psi_-^*,\\
\mathrm{i}\hbar\partial_t\psi_0=&-\frac{\hbar^2}{2m}\partial_x^2\psi_0+V_0(x)\psi_0+(c_0+c_2)(|\psi_+|^2+|\psi_-|^2)\psi_0\\
&+c_0|\psi_0|^2\psi_0+2c_2\psi_+\psi_-\psi_0^*,\\
\mathrm{i}\hbar\partial_t\psi_-=&-\frac{\hbar^2}{2m}\partial_x^2\psi_-+V_-(x)\psi_-+(c_0+c_2)(|\psi_0|^2+|\psi_-|^2)\psi_-\\
&+(c_0-c_2)|\psi_+|^2\psi_-+c_2\psi_0^2\psi_+^*.
\end{aligned} \tag{2}$$

Eqs. (2) are obtained by taking into account the longitudinal components of the wave functions on the transverse plane (y,z) of the coupled three-dimensional GPEs [46–48].

Particularly, we consider the conditions $\hbar=1$, $m=0.5$, $c_0=c_2=-0.5k^2$, rescale the variable by the transformation (ψ_+,ψ_0,ψ_-) to $(\psi_+,\sqrt{2}\psi_0,\psi_-)$, and introduce gain-and-loss distribution $W_j(x)$ ($j=+,0,-$) into Eqs. (2). Consequently, we obtain the dimensionless three-component GPEs under the influence of a $\mathcal{PT}$-symmetric δ-function potential:

$$\begin{aligned}
&\mathrm{i}\psi_{+,t}+\psi_{+,xx}+k^2(|\psi_+|^2+2|\psi_0|^2)\psi_++k^2\psi_0^2\psi_-^*-U_+(x)\psi_+=0,\\
&\mathrm{i}\psi_{0,t}+\psi_{0,xx}+k^2(|\psi_+|^2+|\psi_0|^2+|\psi_-|^2)\psi_0+k^2\psi_+\psi_-\psi_0^*-U_0(x)\psi_0=0,\\
&\mathrm{i}\psi_{-,t}+\psi_{-,xx}+k^2(2|\psi_0|^2+|\psi_-|^2)\psi_-+k^2\psi_0^2\psi_+^*-U_-(x)\psi_-=0,
\end{aligned} \tag{3}$$

where $\psi_j=\psi_j(x,t)$, $U_j(x)=V_j(x)+\mathrm{i}W_j(x)$ ($j=+,0,-$) are complex functions. The subscript denotes the partial derivative with respect to variables and the star denotes the complex conjugate. These equations can describe the spin-1 BECs system, allowing us to explore peakons with three coupled interactions, a topic that has been rarely discussed in previous research. This also confirms that introducing $\mathcal{PT}$-symmetric potentials into unstable systems may lead to the generation of stable nonlinear modes. We conducted a study on stable peakons generated by introducing $\mathcal{PT}$-symmetric δ-function potentials, exploring the patterns of mean-field and spin-exchange interaction in relation to peakon energy variations. This research might contribute to a more comprehensive understanding of nonlinear systems and provide reference for future related experiments.

The remaining structure of this paper is organized as follows: In Section 2, we provide the specific form of the classical δ-function potentials and present the analytical peakon solutions corresponding to Eq. (3). In Section 3, we conduct a analysis of families of analytical solutions, investigating how variations in parameters affect the shape of these curves. Subsequently, we explore the evolution of both stable and unstable peakon solutions corresponding to points on these curves. In Section 4, we extend our analysis beyond analytical solutions by employing the squared-operator iterative algorithms [49] to obtain diverse families of numerical solutions for different nonlinear modes. Similarly, we conduct an analysis of energy curves, as well as the corresponding peakons. In Section 5, we summarize some conclusions.

2. Analytical peakon solutions with $\mathcal{PT}$-symmetric δ-function potentials

In this paper, we choose $\mathcal{PT}$-symmetric δ-function potentials in the form as

$$\begin{aligned}
&V_j(x)=v_j\delta(x),\\
&W_j(x)=w_j\,\mathrm{sgn}(x)\rho_j(x),\qquad j=+,0,-,
\end{aligned} \tag{4}$$

where $\rho_j(x)=\mathrm{e}^{-\lambda_j|x|}$, λ_j, v_j, w_j are all real parameters, and "sgn(x)" denotes the sign function. Next, we focus on the expression form of the stationary solutions given by $\psi_j(x,t)=\boldsymbol{\Phi}_j(x)\mathrm{e}^{\mathrm{i}\mu_jt}$, where $\boldsymbol{\Phi}_j(x)=\phi_j(x)\mathrm{e}^{\mathrm{i}\gamma_j(x)}$ ($j=+,0,-$).

Through the stationary transformation and solving the linear spectrum problem which is simplified with the constraints $\lambda_j=\lambda$, $v_j=v, w_j=w, \mu_j=\lambda^2, V_j(x)=V(x), W_j(x)=W(x)$, as derived subsequently, we obtained the $\mathcal{PT}$-symmetry breaking lines which indicating the stability of the background solution in Fig. 1. We define whether the max imaginary part of background eigenvalues is greater than 10^{-5} to distinguish between $\mathcal{PT}$-broken and $\mathcal{PT}$-unbroken. In Fig. 1(a), it can be observed that the domains of unbroken get larger with the increase of λ. The red dashed line represents the case of $\lambda=0.35$, where region I is $\mathcal{PT}$-unbroken, regions II and III are $\mathcal{PT}$-broken. The blue solid line represents the case of $\lambda=1.8$, where regions I and II are $\mathcal{PT}$-unbroken, region III is $\mathcal{PT}$-broken. In Fig. 1(b), we select the case of $\lambda=-0.5v$ for analysis. $\mathcal{PT}$-unbroken region IV and $\mathcal{PT}$-broken region V precisely corresponding to the situation depicted in Fig. 2(a). We marked the positions corresponding to points A, B, C, and D in Fig. 2(a) on Fig. 1(b), allowing a clear visualization that points B, C are $\mathcal{PT}$-unbroken, while points A, D are $\mathcal{PT}$-broken. Furthermore, in Table 1, we provide the stability of the background solutions corresponding to the points mentioned in this paper.

To obtain nonlinear modes in Eqs. (3) with assumed condition $2\mu_0=\mu_++\mu_-$, we can derive the stationary form as

$$\begin{aligned}
&-\mu_++\frac{\phi_{+,xx}}{\phi_+}-\gamma_{+,x}^2+\mathrm{i}\gamma_{+,xx}+2\mathrm{i}\gamma_{+,x}\frac{\phi_{+,x}}{\phi_+}+k^2(\phi_+^2+2\phi_0^2)+k^2\phi_0^2\frac{\phi_-}{\phi_+}-U_+(x)=0,\\
&-\mu_0+\frac{\phi_{0,xx}}{\phi_0}-\gamma_{0,x}^2+\mathrm{i}\gamma_{0,xx}+2\mathrm{i}\gamma_{0,x}\frac{\phi_{0,x}}{\phi_0}+k^2(\phi_+^2+\phi_0^2+\phi_-^2)+k^2\phi_+\phi_--U_0(x)=0,\\
&-\mu_-+\frac{\phi_{-,xx}}{\phi_-}-\gamma_{-,x}^2+\mathrm{i}\gamma_{-,xx}+2\mathrm{i}\gamma_{-,x}\frac{\phi_{-,x}}{\phi_-}+k^2(2\phi_0^2+\phi_-^2)+k^2\phi_0^2\frac{\phi_+}{\phi_-}-U_-(x)=0.
\end{aligned} \tag{5}$$

Furthermore, considering the result under $\phi_0^2(x)=\phi_+(x)\phi_-(x)$, where the parameters satisfy the relationship $\mu_j=\lambda_j^2$, $\lambda_j=\lambda$, $v_j=v=-2\lambda$, we obtain the analytical expression form of the desired solutions, reading as

$$\begin{aligned}
&\rho_j(x)=\rho(x)=\mathrm{e}^{-\lambda|x|},\\
&\phi_j(x)=A_j\rho(x),\\
&\gamma_j(x)=\frac{w}{3\lambda^2}\,\mathrm{sgn}(x)[\rho(x)-1],\\
&w_j=w=-3k\lambda(A_++A_-),\qquad j=+,0,-,
\end{aligned} \tag{6}$$

where k denotes the equation parameter in Eqs. (3), $A_0^2=A_+A_-$, and in fact, $\gamma_j(x)=\int^x\phi_j(s)ds$. The peakon solutions we obtained have finite-order weak derivatives at the peak point due to the property of the δ-function.

The linear stability of the nonlinear modes is a critical indicator to measure the properties of the solutions. We substitute the perturbed solutions $\psi_j(x,t)$ into Eqs. (3), in the form

$$\psi_j(x,t)=\phi_j(x)\mathrm{e}^{\mathrm{i}\gamma_j(x)}\mathrm{e}^{\mathrm{i}\mu_jt}+\epsilon\left[f_j(x)\mathrm{e}^{\mathrm{i}\delta t}+g_j^*(x)\mathrm{e}^{-\mathrm{i}\delta^*t}\right]\mathrm{e}^{\mathrm{i}\mu_jt},\quad j=+,0,-, \tag{7}$$

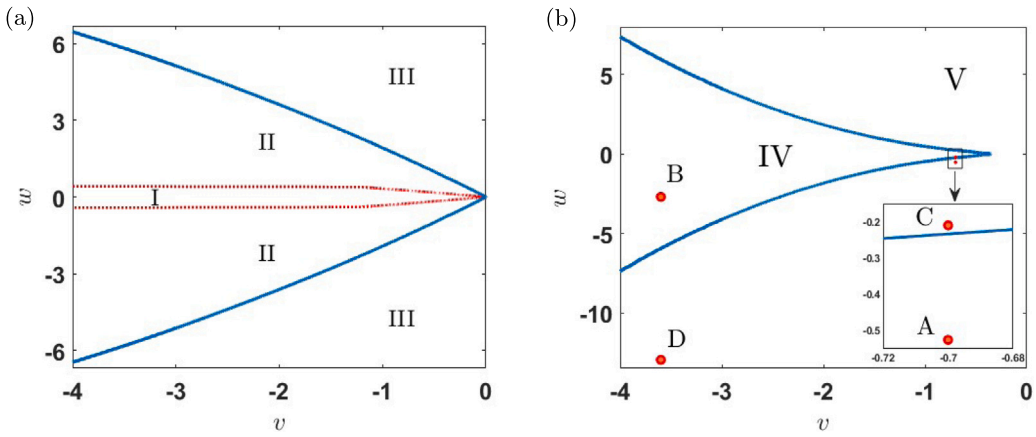

Fig. 1. The domains of broken/unbroken linear $\mathcal{PT}$-symmetric phases. (a) The red dashed line indicates the case of $\lambda = 0.35$, and the blue solid line indicates the case of $\lambda = 1.8$. (b) The blue solid line indicates the case of $\lambda = -0.5v$.

Table 1
Stability of the background solutions corresponding to the points mentioned in this paper.

Figure	Fig. 2				Fig. 4		Fig. 6	
Point corresponds to peakon solution	A	B	C	D	F	G	Q_1	Q_2
Max imaginary part of background eigenvalues	0.0812	9.0×10^{-15}	9.3×10^{-8}	0.0883	2.7×10^{-12}		7.8×10^{-15}	
$\mathcal{PT}$-broken/unbroken (background stability)	broken	unbroken	unbroken	broken	unbroken		unbroken	
Peakon stability	unstable	stable	stable	unstable	stable	unstable	stable	stable

where $\epsilon \ll 1$, and $f_j(x)$, $g_j(x)$ are components of the corresponding eigenfunction. We can obtain the corresponding linear eigenvalue problem. The eigenvalues determine the linear stability of the solutions $\psi_j(x,t)$. If all imaginary parts of eigenvalues are less than 10^{-5}, we consider the solutions to be linearly stable; otherwise, they are linearly unstable. We use the Fourier collocation method in our numerical simulation to discretize the corresponding differential operator into a matrix. By appropriately choosing parameters in the numerical method, the spectrum of the discretization matrix, which is solvable, serves as a reliable approximation for that of the original differential operator. Additionally, in this paper, we investigate the stability of nonlinear modes by numerically evolving them with 5% perturbations as the initial condition in the evolutionary program of peakons.

3. Families of analytical peakon solutions

We use $P_j = \int(|\Phi_j|^2/2)dx$ to represent the energy of the solutions, introducing the Poynting vector $S_j = \mathrm{i}(\Phi_j\Phi^*_{j,x} - \Phi^*_j\Phi_{j,x})/2$, and the total number flux through the origin $J = \sum \mathrm{i}(\Phi^*_j\Phi_{j,x} - \Phi_j\Phi^*_{j,x})\big|_{x=0}$ to describe energy flux [50], where Φ_j $(j = +,0,-)$ denotes the stationary peakon solution. Based on the previously mentioned method of introducing δ-function external potentials in spin-1 BECs for analytically modulating peakons, we employ the constraints expressed by Eqs. (6) and the form of the solutions to plot the families of analytical peakon solutions with the energy of analytical peakons and the external potential parameter λ as coordinate axes. We can easily obtain energy curves for analytical peakons with different amplitudes. For the sake of clarity, here we take the curve that satisfies the maximum amplitude consistency $|A_j| = |A|$, $P_j = P$ $(j = +,0,-)$, as an example.

Under the condition of $k = 1$ for the three-coupled GPEs, we obtain the family of analytical peakon solutions illustrated in Fig. 2(a) using a solid line, all with $|A| = 0.25$, and select two points A, B on the curve for further analysis. Point A corresponds to $\lambda = 0.35$, $P = 0.7280$, and point B corresponds to $\lambda = 1.8$, $P = 0.1438$. The evolutionary results of the two sets of peakons represented by points A, B, after undergoing 5% perturbations as the initial condition, are depicted in Figs. 2(b1)–(b3) and 2(c1)–(c3), respectively. Point A corresponds to an unstable situation, while point B corresponds to a stable one, and their eigenvalue distributions are also reflected in Figs. 2(b4) and 2(c4).

Under the condition of unchanged parameters, changing only $|A|$ of the modulated peakon solutions can affect the stability of the resulting peakons. Points C and D in Fig. 2(a) illustrate this phenomenon. Point C, relative to point A, corresponds to peakon solutions with $k = 1$, $\lambda = 0.35$, remaining unchanged, but the amplitude decreases from $|A| = 0.25$ to $|A| = 0.1$, and the energy decreases from $P = 0.7280$ to $P = 0.1165$, resulting in stability. Conversely, point D, relative to point B, corresponds to peakon solutions with $k = 1$, $\lambda = 1.8$, remaining unchanged, but the amplitude increases from $|A| = 0.25$ to $|A| = 1.2$, and the energy increases from $P = 0.1438$ to $P = 3.3123$, resulting in instability. Furthermore, as depicted by the dashed lines in Fig. 2(a), point C can be viewed as a point on the curve of analytical peakon solutions with $|A| = 0.1$, and point D can be viewed as a point on the curve of analytical peakon solutions with $|A| = 1.2$.

We investigate the relationship between J and w under the condition $w_j = w$, and the results are shown in Fig. 3. In Fig. 3(a), we consider the case satisfying the analytical conditions $k = 1$, $\lambda_+ = \lambda_0 = \lambda_- = \lambda$, $A_+ = A_0 = A_- = -w/6\lambda$. The blue solid line represents $\lambda = 1.8$, and the red dashed line represents $\lambda = 0.35$, corresponding to the total number flux at points A, B, C, and D in Fig. 2(a). Furthermore, we conduct a study on the total number flux from the numerical solutions. The points corresponding to F, G, Q_1, Q_2 on Figs. 4(a1) and 6(a1) are marked in Fig. 3(b)–(c). In Fig. 3(b), $k = 1$, $\lambda_+ = 1$, $\lambda_0 = 0.7$, $\lambda_- = 1.2$, $v_+ = -3$, $v_0 = -2.1$, $v_- = -3.6$. The blue solid line represents $P_+ = 1$, $P_0 = 0.01$, $P_- = 2.99$, and the red dashed line represents

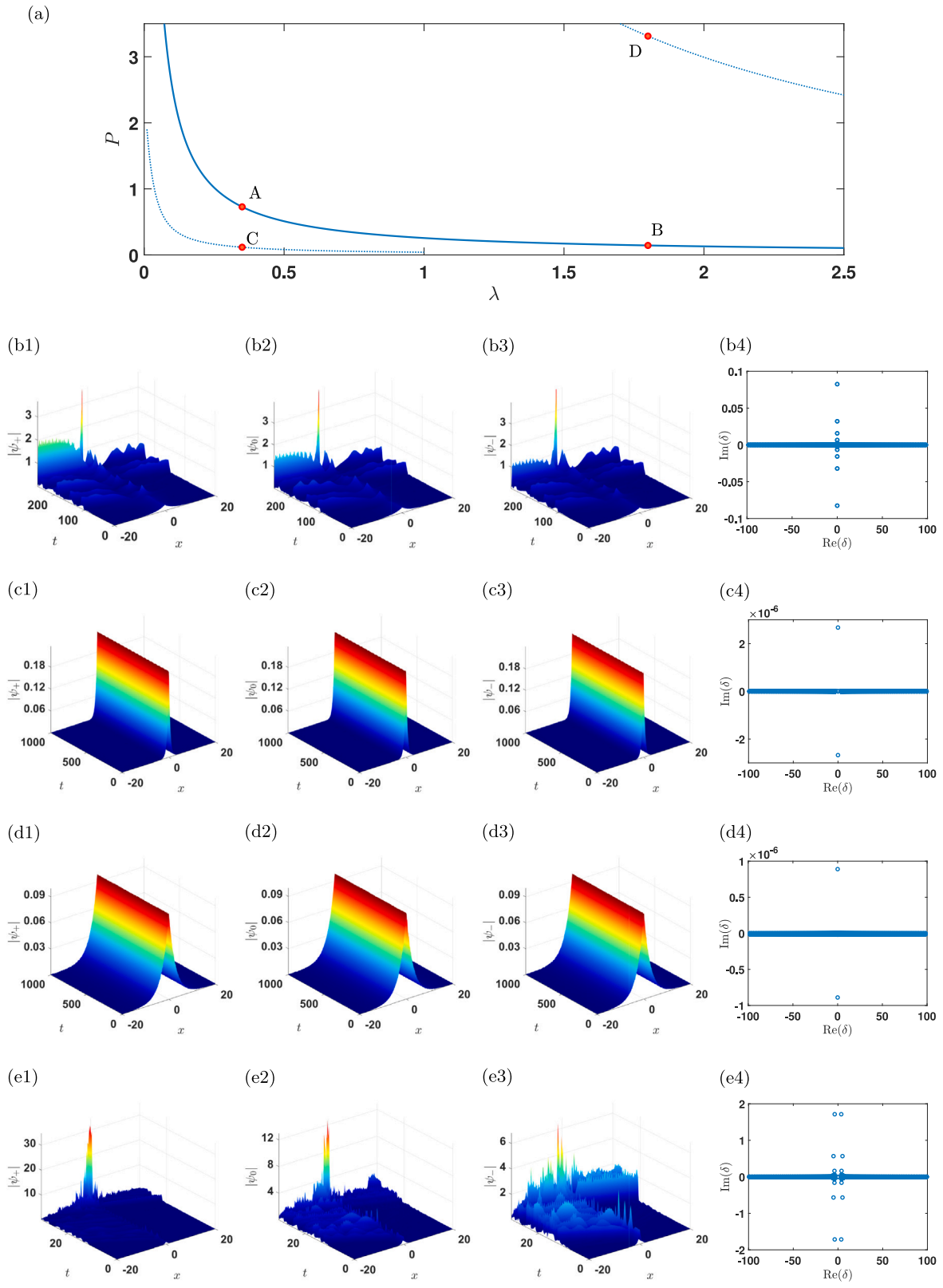

Fig. 2. Families of analytical peakons and their evolution. (a) Families of analytical peakons with coordinates P and λ. (b1)–(b4) The evolution of unstable analytical peakons corresponding to point A in (a) and their linear stability eigenvalues. (c1)–(c4) The evolution of stable analytical peakons corresponding to point B in (a) and their linear stability eigenvalues. (d1)–(d4) The evolution of stable analytical peakons corresponding to point C in (a) and their linear stability eigenvalues. (e1)–(e4) The evolution of unstable analytical peakons corresponding to point D in (a) and their linear stability eigenvalues. Maximum amplitudes are chosen as $|A_+| = |A_0| = |A_-| = |A|$. Point A corresponds to $k = 1$, $\lambda = 0.35$, $P = 0.7280$, $|A| = 0.25$; point B corresponds to $k = 1$, $\lambda = 1.8$, $P = 0.1438$, $|A| = 0.25$; point C corresponds to $k = 1$, $\lambda = 0.35$, $P = 0.1165$, $|A| = 0.1$; point D corresponds to $k = 1$, $\lambda = 1.8$, $P = 3.3123$, $|A| = 1.2$.

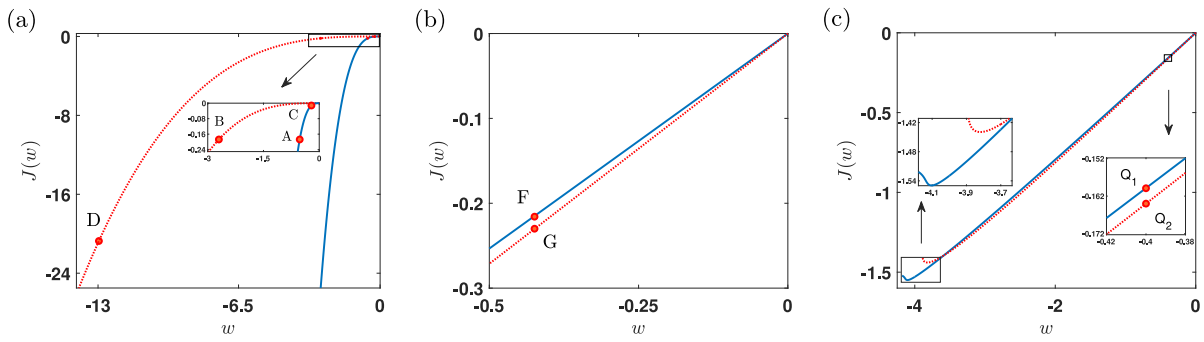

Fig. 3. The total number flux through the origin. (a) J with the analytical solutions. The parameters are $k = 1$, $\lambda_+ = \lambda_0 = \lambda_- = \lambda$, $A_+ = A_0 = A_- = -w/6\lambda$. The blue solid line represents $\lambda = 1.8$, and the red dashed line represents $\lambda = 0.35$. (b) J with the numerical solutions. The parameters are $k = 1$, $\lambda_+ = 1$, $\lambda_0 = 0.7$, $\lambda_- = 1.2$, $v_+ = -3$, $v_0 = -2.1$, $v_- = -3.6$. The blue solid line represents $P_+ = 1$, $P_0 = 0.01$, $P_- = 2.99$, and the red dashed line represents $P_+ = 0.5$, $P_0 = 1.51$, $P_- = 1.99$. (c) J with the numerical solutions. The parameters are $k = 1$, $\lambda_+ = 1$, $\lambda_0 = 1.3$, $\lambda_- = 1.2$, $v_+ = -2$, $v_0 = -2.6$, $v_- = -2.4$. The blue solid line represents $P_+ = 0.4285$, $P_0 = 0.7380$, $P_- = 2.0335$, and the red dashed line represents $P_+ = 1.8615$, $P_0 = 0.7380$, $P_- = 0.6005$.

$P_+ = 0.5$, $P_0 = 1.51$, $P_- = 1.99$. In Fig. 3(c), $k = 1$, $\lambda_+ = 1$, $\lambda_0 = 1.3$, $\lambda_- = 1.2$, $v_+ = -2$, $v_0 = -2.6$, $v_- = -2.4$. The blue solid line represents $P_+ = 0.4285$, $P_0 = 0.7380$, $P_- = 2.0335$, and the red dashed line represents $P_+ = 1.8615$, $P_0 = 0.7380$, $P_- = 0.6005$. In Fig. 3(a)–(b) the variation of J with w appears normal. However, in Fig. 3(c), the variation of J with w appears anomalous when the parameter w near the $\mathcal{PT}$-broken/unbroken boundary.

4. Families of numerical peakon solutions

Since BECs can be implemented experimentally using physical methods such as Feshbach resonance imposed by tightly focused laser beams [51], it becomes more practically relevant to describe the system parameters for the three coupled GPEs and the families of peakon solutions. Besides, the above solutions obtained through the analytical method have various constraints between parameters and variables. Based on this, in order to remove the constraint conditions and change the propagation coefficients, we further derived other fundamental peakons using numerical methods. Here, we generalize the coefficients of the cubic terms $|\psi_+|^2\psi_+$, $|\psi_0|^2\psi_+$, and $|\psi_-|^2\psi_+$ in the first equation of Eqs. (3) from k^2, $2k^2$, 0 to a_+, a_0, a_- for the purpose of our study. We employ the power-conserving squared-operator iterative algorithms to obtain families of nonlinear modes and plot the energy curves with the energy of numerical solutions and the propagation coefficient as coordinate axes. By using the linear stability analysis method described in the previous section, we can easily determine the stability of each point on the energy curves. Similarly, the evolution with 5% perturbations is performed.

To investigate the influence of different parameters on the families of nonlinear modes, we take the representative curve with P_+ and μ_+ as the coordinate axes, shown in Fig. 4(a1), as the baseline and use the method of controlling variables to study the influence of parameters λ_+, a_+, a_0, and a_-, which are most closely related to it. The parameters of the baseline are chosen as $a_+ = 1$, $a_0 = 2$, $a_- = 0$, $k = 1$, $\lambda_+ = 1$, $\lambda_0 = 0.7$, $\lambda_- = 1.2$, $v_+ = -3$, $v_0 = -2.1$, $v_- = -3.6$, $w_+ = w_0 = w_- = -0.3\sqrt{2}$. Furthermore, Fig. 4(a2)–(a5) illustrate the families of nonlinear modes under the variation of parameters.

As λ_+ increases, the entire curve shifts towards larger μ_+ values. Increasing a_+ causes the most significant change in the curve by moving the upper prominent point towards larger μ_+ values in a substantial manner, while the lower prominent point moves slightly, and the lower endpoint shows no significant change. Increasing a_0 causes the upper and lower prominent points to move towards larger μ_+ values, expanding the range of μ_+ values covered by the curve. The variation of a_-, to a certain extent, even leads to a change in the direction of prominence of the curve.

It is worth noting that on the curve shown in Fig. 4(a1), one μ_+ can correspond to multiple different P_+ values. This means that under the same propagation coefficient condition, we can obtain multiple solutions with different energy. In this case, the other two propagation coefficients may be different. In addition, we selected points F and G on the curve shown in Fig. 4(a1) for further study. Point F corresponds to $P_+ = 1$, $P_0 = 0.01$, $P_- = 2.99$, $\mu_+ = 2.2724$, $\mu_0 = 2.0166$, $\mu_- = 3.6344$; point G corresponds to $P_+ = 0.5$, $P_0 = 1.51$, $P_- = 1.99$, $\mu_+ = 3.2343$, $\mu_0 = 1.8666$, $\mu_- = 4.1068$. By evolving the nonlinear modes corresponding to these two points, we obtained their evolution and energy flux in Fig. 4(b1)–(d3). It is evident that point F corresponds to a stable situation, whereas point G corresponds to an unstable scenario. By applying the stability analysis method mentioned in the previous section, we can determine the stability of each point on the families of nonlinear modes and validate it through the evolution of the nonlinear modes.

Due to the fact that 'long' impurities may act as centers of spontaneous nucleation of solitons [52], to investigate the interaction of free-standing solitons with impurities, we can consider the obtained stationary peakons as 'long' impurities in space. In this paper, we choose Gaussian solitons as outside exotic solitons and considered the following initial conditions

$$\overline{\psi_j}(x,0) = \psi_j(x,0) + q_j e^{-0.05(x+25)^2+3ix}, \qquad j = +,0,-, \tag{8}$$

where q_j represents the modulus of Gaussian soliton. Fig. 5(a1)–(b3) correspond to analytical peakons at $k = 1, \lambda = 1.8, P = 0.1438, |A| = 0.25$ (representing the situation depicted in Fig. 2(c1)–(c3)), while Fig. 5(c1)–(c3) correspond to numerical peakons at $P_+ = 1$, $P_0 = 0.01$, $P_- = 2.99$, $\mu_+ = 2.2724$, $\mu_0 = 2.0166$, $\mu_- = 3.6344$ (representing the situation depicted in Fig. 4(c1)–(c3)). For Fig. 5(a1)–(a3), we choose $q_+ = q_0 = q_- = 0.25$. For Fig. 5(b1)–(b3), $q_+ = 0.05, q_0 = 0.25, q_- = 1.25$, and for Fig. 5(c1)–(c3), $q_+ = q_0 = q_- = 0.5$. We can observe that after the interaction between solitons and peakons, a portion of the solitons continue to propagate forward along their original direction, while another parts are 'reflected' back, propagating along the 'mirror' direction.

Similarly, we can apply the same analysis to the two groups of families of nonlinear modes formed by (μ_0, P_0) and (μ_-, P_-). On the curve with P_0 and μ_0 as the coordinate axes, we discover a closed-loop structure resembling the number "8" lying on its side, as shown in Fig. 6(a2), where the coordinates of points M, N, Q are respectively (2.1826,0.2211), (2.3035,0.010), (2.2496,0.7380). This indicates that the point Q on Fig. 6(a2) corresponds to two points Q1 and Q2 on Fig. 6(a1) or Fig. 6(a3), namely two sets of nonlinear modes with identical energy P_0 and propagation coefficient μ_0, but with different P_+, P_-, μ_+, and μ_- values. The parameters for these families of numerical peakon solutions are chosen as $k = 1$, $\lambda_+ = 1$, $\lambda_0 = 1.3$,

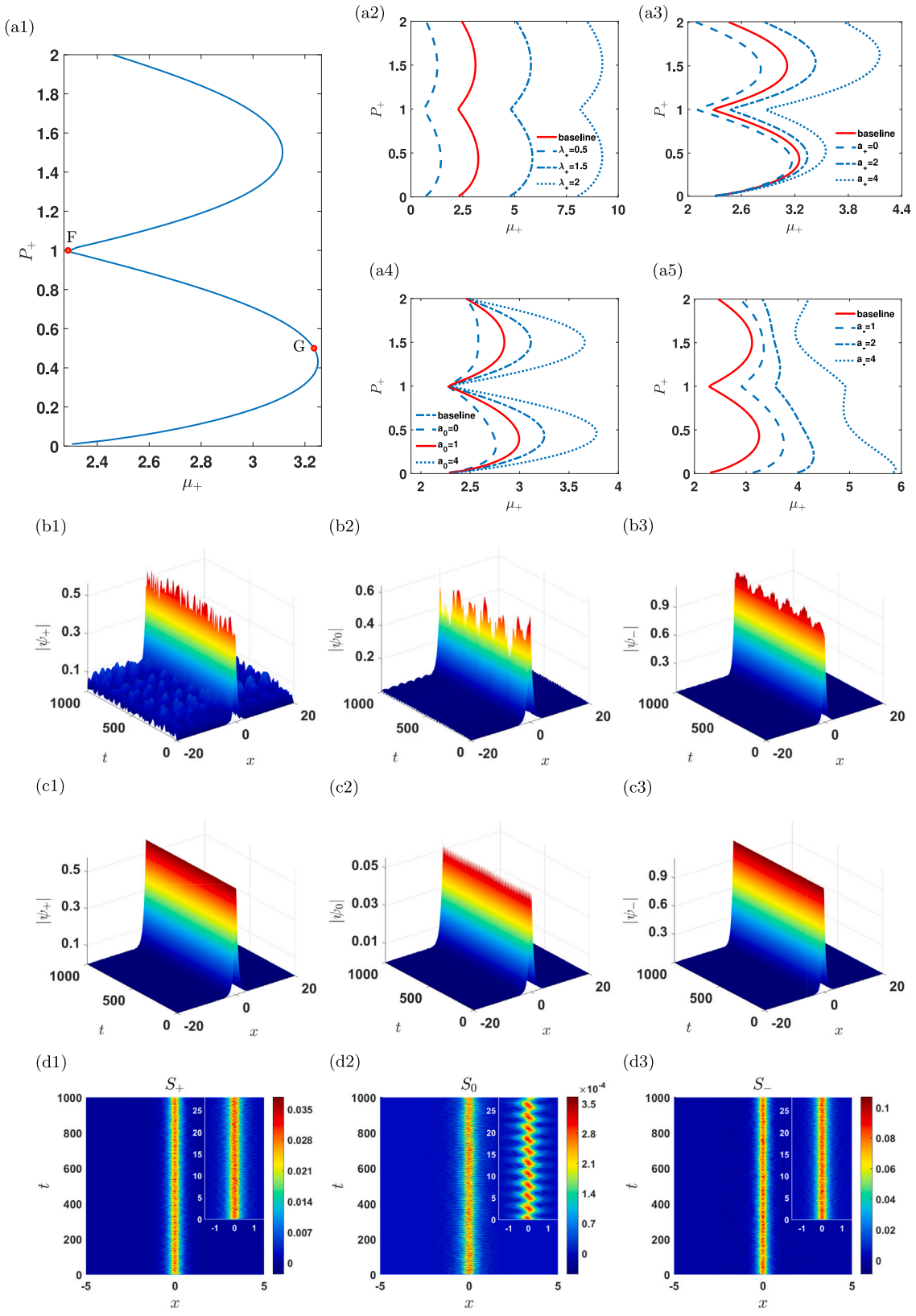

Fig. 4. Families of numerical peakons and their evolution. (a1) Families of numerical peakons with coordinates P_+ and μ_+, which is used as a baseline for subsequent analysis. (a2)–(a5) Families of nonlinear modes and the impacts of the parameters. (b1)–(b3) The evolution of unstable numerical peakons corresponding to point G in (a1). (c1)–(d3) The evolution of stable numerical peakons and their energy flux corresponding to point F in (a1). The parameters for the baseline are chosen as $a_+ = 1$, $a_0 = 2$, $a_- = 0$ ($k = 1$), $\lambda_+ = 1$, $\lambda_0 = 0.7$, $\lambda_- = 1.2$, $v_+ = -3$, $v_0 = -2.1$, $v_- = -3.6$, $w_+ = w_0 = w_- = -0.3\sqrt{2}$. Point F corresponds to $P_+ = 1$, $P_0 = 0.01$, $P_- = 2.99$, $\mu_+ = 2.2724$, $\mu_0 = 2.0166$, $\mu_- = 3.6344$; point G corresponds to $P_+ = 0.5$, $P_0 = 1.51$, $P_- = 1.99$, $\mu_+ = 3.2343$, $\mu_0 = 1.8666$, $\mu_- = 4.1068$.

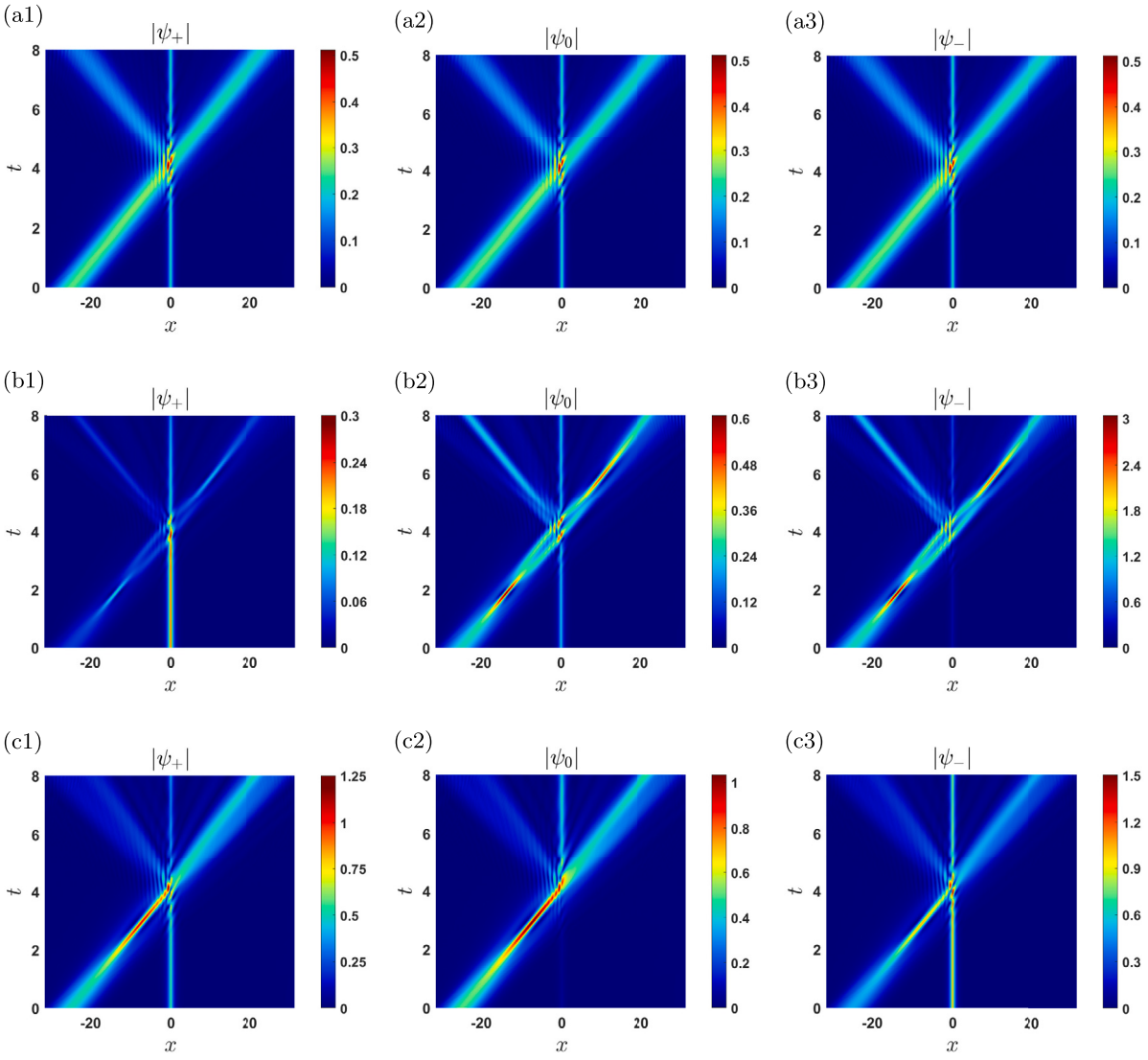

Fig. 5. Interactions of Gaussian solitons with peakon impurities. (a1)–(b3) correspond to analytical peakons at $k = 1, \lambda = 1.8, P = 0.1438, |A| = 0.25$, while (c1)–(c3) correspond to numerical peakons at $P_+ = 1$, $P_0 = 0.01$, $P_- = 2.99$, $\mu_+ = 2.2724$, $\mu_0 = 2.0166$, $\mu_- = 3.6344$. For (a1)–(a3), $q_+ = q_0 = q_- = 0.25$. For (b1)–(b3), $q_+ = 0.05$, $q_0 = 0.25, q_- = 1.25$. For (c1)–(c3), $q_+ = q_0 = q_- = 0.5$.

$\lambda_- = 1.2$, $v_+ = -2$, $v_0 = -2.6$, $v_- = -2.4$, $w_+ = w_0 = w_- = -0.4$. Figs. 6(b1)–(c3) and 6(d1)–(d3) correspond to two distinct sets of peakon solutions of point Q in Fig. 6(a2). Two sets of peakon solutions correspond to the same energy and propagation coefficient for ψ_0, namely $P_0 = 0.7380$ and $\mu_0 = 2.2496$. However, for the parameters describing ψ_+ and ψ_-, Figs. 6(b1)–(c3) and 6(d1)–(d3) correspond to the cases of $P_+ = 0.4285$, $P_- = 2.0335$, $\mu_+ = 1.4713$, $\mu_- = 1.9661$ (point Q_1) and $P_+ = 1.8615$, $P_- = 0.6005$, $\mu_+ = 1.4803$, $\mu_- = 1.8877$ (point Q_2), respectively. Furthermore, as shown in Figs. 6(b1)–(b3) and 6(d1)–(d3), these two peakons exhibit evident periodic behavior during their evolution, which can be regarded as a manifestation of internal energy transfer within the coupled system.

5. Conclusion

By introducing $\mathcal{PT}$-symmetric δ-function potentials into three-component GPEs that describe spinor $F = 1$ BECs, we obtain both stable and unstable analytical peakon solutions. These solutions allow us to explore the patterns of mean-field and spin-exchange interactions as they relate to variations in the energy of nonlinear modes, which also proves the significance of $\mathcal{PT}$-symmetric potentials in manipulating nonlinear interactions. Furthermore, through the utilization of iterative algorithms, we generate a series of numerical solutions and represent various families of peakons in the form of energy curves. This approach helps us understand the influence of parameters on these curves. Moreover, we make a noteworthy observation of an intriguing closed-loop structure within the family of peakons, with P_0 and μ_0 serving as the coordinate axes. Point Q on this curve corresponds to two sets of nonlinear modes with identical energy P_0 and propagation coefficient μ_0, but with different values for P_+, P_-, μ_+, and μ_-. After undergoing evolution with 5% perturbations applied as the initial condition, we confirm the stability of these two sets of peakons and observe distinct periodic oscillatory properties, which can be considered as an indication of internal energy transfer within the coupled system.

In summary, we offer a new perspective on the behavior of peakons in spin-1 BECs system with $\mathcal{PT}$-symmetric potentials, which might contribute to a more comprehensive understanding of coupled nonlinear systems and serve as a reference for future experiments in this domain.

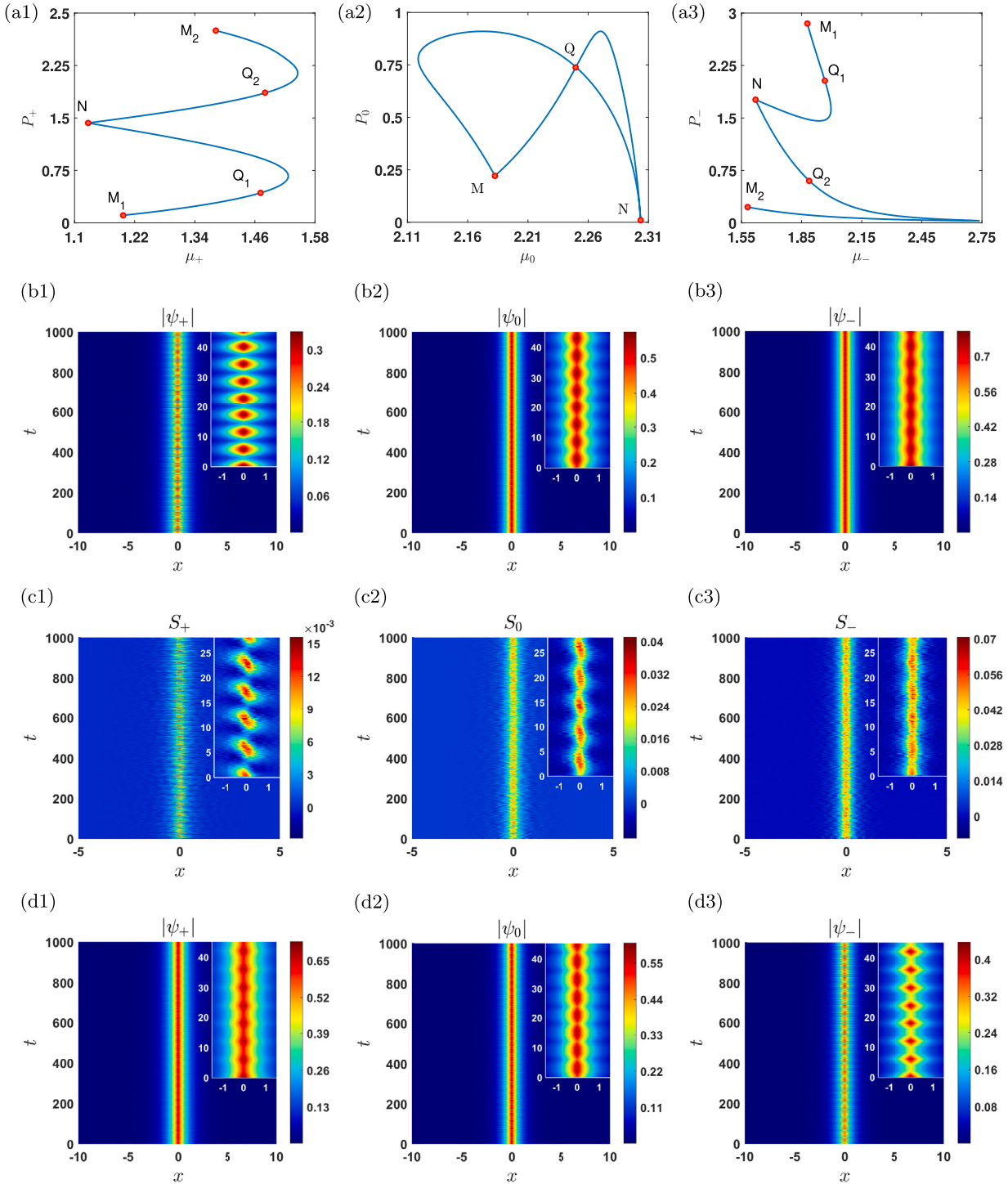

Fig. 6. Families of numerical peakons and their evolution. (a1)–(a3) Families of numerical peakons with coordinates P_j and μ_j $(j = +, 0, -)$, and the point Q corresponds to two distinct sets of peakon solutions. (b1)–(c3) The evolution of stable numerical peakons and their energy flux corresponding to point Q in (a2) (point Q_1 in (a1) and (a3)). (d1)–(d3) The evolution of another group of stable numerical peakons corresponding to point Q in (a2) (point Q_2 in (a1) and (a3)). The parameters are chosen as $k = 1$, $\lambda_+ = 1$, $\lambda_0 = 1.3$, $\lambda_- = 1.2$, $v_+ = -2$, $v_0 = -2.6$, $v_- = -2.4$, $w_+ = w_0 = w_- = -0.4$. (b1)–(c3) correspond to $P_+ = 0.4285$, $P_0 = 0.7380$, $P_- = 2.0335$, $\mu_+ = 1.4713$, $\mu_0 = 2.2496$, $\mu_- = 1.9661$; (d1)–(d3) correspond to $P_+ = 1.8615$, $P_0 = 0.7380$, $P_- = 0.6005$, $\mu_+ = 1.4803$, $\mu_0 = 2.2496$, $\mu_- = 1.8877$.

CRediT authorship contribution statement

Jun-Yi Lao: Writing – original draft, Software. **Zi-Yang Qin:** Software. **Jia-Rui Zhang:** Software. **Yu-Jia Shen:** Writing – review & editing, Supervision.

Declaration of competing interest

The authors declare that they have no known competing financial interests or personal relationships that could have appeared to influence the work reported in this paper.

Data availability

No data was used for the research described in the article.

Acknowledgments

We express our sincere thanks to the editor, referees, and all the members of our discussion group for their valuable comments. This work was supported by NSFC under Grant number 12272403, and Beijing Training Program of Innovation (Grant number S202310019091). The funding body plays an important role in the design of the study, in analysis, calculation, and in writing of the manuscript.

Funding

This work was supported by NSFC under Grant number 12272403, and Beijing Training Program of Innovation (Grant number S202310019091). The funding body plays an important role in the design of the study, in analysis, calculation, and in writing of the manuscript.

References

[1] Aveline DC, Williams JR, Elliott ER, Dutenhoffer C, Kellogg JR, Kohel JM, et al. Observation of Bose-Einstein condensates in an Earth-orbiting research lab. Nature 2020;582:193–7.
[2] Nodari SR, Conforti M, Dujardin G, Kudlinski A, Mussot A, Trillo S, et al. Modulational instability in dispersion-kicked optical fibers. Phys Rev A 2015;92:013810.
[3] Miao Y, Ilievski E, Gamayun O. Interplay of solitons and radiation in one-dimensional Bose gases. Phys Rev A 2019;99:023605.
[4] Watabe S. Hugenholtz-Pines theorem for multicomponent Bose-Einstein condensates. Phys Rev A 2021;103:053307.
[5] Zhang J-R, Zhang J-Q, Zheng Z-L, Lin D, Shen Y-J. Dynamic behavior and stability analysis of nonlinear modes in the fourth-order generalized Ginzburg-Landau model with near $\mathcal{PT}$-symmetric potentials. Nonlinear Dyn 2022;109:1005–17.
[6] Konotop VV, Yang J, Zezyulin DA. Nonlinear waves in $\mathcal{PT}$-symmetric systems. Rev Modern Phys 2016;88:035002.
[7] Feng B-F, Luo X-D, Ablowitz MJ, Musslimani ZH. General soliton solution to a nonlocal nonlinear Schrödinger equation with zero and nonzero boundary conditions. Nonlinearity 2017;31:5385–409.
[8] Ablowitz MJ, Feng B-F, Luo X-D, Musslimani ZH. Reverse space-time nonlocal Sine-Gordon/Sinh-Gordon equations with nonzero boundary conditions. Stud Appl Math 2018;141:267–307.
[9] Yang B, Yang J. Transformations between nonlocal and local integrable equations. Stud Appl Math 2018;140:178–201.
[10] Hang C, Huang G, Konotop VV. $\mathcal{PT}$ Symmetry with a system of three-level atoms. Phys Rev Lett 2013;110:083604.
[11] Boettcher F, Schmidt J-N, Hertkorn J, Ng KSH, Graham SD, Guo M, et al. New states of matter with fine-tuned interactions: quantum droplets and dipolar supersolids. Rep Progr Phys 2021;84:012403.
[12] Baranov MA, Dalmonte M, Pupillo G, Zoller P. Condensed matter theory of dipolar quantum gases. Chem Rev 2012;112:5012–61.
[13] Meng Z, Wang L, Han W, Liu F, Wen K, Gao C, et al. Atomic Bose-Einstein condensate in twisted-bilayer optical lattices. Nature 2023;615:231–6.
[14] Li L, Li Z, Malomed BA, Mihalache D, Liu WM. Exact soliton solutions and nonlinear modulation instability in spinor Bose-Einstein condensates. Phys Rev A 2005;72:033611.
[15] Ieda J, Miyakawa T, Wadati M. Exact analysis of soliton dynamics in spinor Bose-Einstein condensates. Phys Rev Lett 2004;93:194102.
[16] Li S, Prinari B, Biondini G. Solitons and rogue waves in spinor Bose-Einstein condensates. Phys Rev E 2018;97:022221.
[17] Kengne E, Liu W-M, Malomed BA. Spatiotemporal engineering of matter-wave solitons in Bose-Einstein condensates. Phys Rep 2021;899:1–62.
[18] Liu K, He H, Zhang Y. Raman-induced spin-orbit-coupled and spin-tensor-momentum-coupled spin-1 Bose-Einstein condensates in a toroidal trap. Phys Lett A 2022;448:128330.
[19] Lin Y-J, Compton RL, Perry AR, Phillips WD, Porto JV, Spielman IB. Bose-Einstein condensate in a uniform light-induced vector potential. Phys Rev Lett 2009;102:130401.
[20] Fialko O, Brand J, Zülicke U. Soliton magnetization dynamics in spin-orbit-coupled Bose-Einstein condensates. Phys Rev A 2012;85:051605.
[21] Tian L, Zheng N, Jian J, Liu W, Wu J, Li Y, et al. Spin current in a spinor Bose-Einstein condensate induced by a gradient magnetic field. Chin Phys B 2022;31:110302.
[22] Stamper-Kurn DM, Ueda M. Spinor Bose gases: Symmetries, magnetism, and quantum dynamics. Rev Modern Phys 2013;85:1191–244.
[23] Adhikari SK. Vortex-lattice formation in a spin-orbit coupled rotating spin-1 condensate. J Phys: Condens Matter 2020;33:065404.
[24] Campbell DL, Price RM, Putra A, Valdes-Curiel A, Trypogeorgos D, Spielman IB. Magnetic phases of spin-1 spin-orbit-coupled Bose gases. Nature Commun 2016;7:013810.
[25] Tylutki M, Astrakharchik GE, Malomed BA, Petrov DS. Collective excitations of a one-dimensional quantum droplet. Phys Rev A 2020;101:051601.
[26] Chomaz L, Baier S, Petter D, Mark MJ, Wächtler F, Santos L, et al. Quantum-fluctuation-driven crossover from a dilute Bose-Einstein condensate to a macrodroplet in a dipolar quantum fluid. Phys Rev X 2016;6:041039.
[27] Aikawa K, Frisch A, Mark M, Baier S, Rietzler A, Grimm R, et al. Bose-Einstein condensation of erbium. Phys Rev Lett 2012;108:210401.
[28] Gallone M. Self-adjoint extensions of Dirac operator with Coulomb potential. In: Advances in quantum mechanics: contemporary trends and open problems. vol. 18, 2017, p. 169–85.
[29] Holmer J, Marzuola J, Zworski M. Fast soliton scattering by delta impurities. Comm Math Phys 2007;274:187–216.
[30] Suchkov SV, Sukhorukov AA, Huang J, Dmitriev SV, Lee C-K, Kivshar YS. Nonlinear switching and solitons in $\mathcal{PT}$-symmetric photonic systems. Laser Photonics Rev 2015;10:177–213.
[31] Chen Y, Yan Z, Mihalache D. Stable flat-top solitons and peakons in the $\mathcal{PT}$-symmetric δ-signum potentials and nonlinear media. Chaos 2019;29:083108.
[32] Bender CM, Boettcher S. Real spectra in non-Hermitian Hamiltonians having $\mathcal{PT}$ symmetry. Phys Rev Lett 1998;80:5243–6.
[33] Mayteevarunyoo T, Malomed BA, Reoksabutr A. Solvable model for solitons pinned to a parity-time-symmetric dipole. Phys Rev E 2013;88:022919.
[34] Wang L, Malomed BA, Yan Z. Attraction centers and parity-time-symmetric delta-functional dipoles in critical and supercritical self-focusing media. Phys Rev E 2019;99:052206.
[35] Karjanto N, Hanif W, Malomed BA, Susanto H. Interactions of bright and dark solitons with localized $\mathcal{PT}$-symmetric potentials. Chaos 2015;25:023112.
[36] Kirikchi OB, Karjanto N. Discrete solitons dynamics in $\mathcal{PT}$-symmetric oligomers with complex-valued couplings. Nonlinear Dyn 2021;103:2769.
[37] Gomez-Gardeñes J, Malomed BA, Floría LM, Bishop AR. Solitons in the Salerno model with competing nonlinearities. Phys Rev E 2006;73:036608.
[38] Cai D, Bishop AR, Grønbech-Jensen N. Perturbation theories of a discrete, integrable nonlinear Schrödinger equation. Phys Rev E 1996;53:4131–6.
[39] Sykes AG, Davis MJ, Roberts DC. Drag force on an impurity below the superfluid critical velocity in a quasi-one-dimensional Bose-Einstein condensate. Phys Rev Lett 2009;103:085302.
[40] Morgan SA. Response of Bose-Einstein condensates to external perturbations at finite temperature. Phys Rev A 2004;69:023609.
[41] Barashenkov IV, Zezyulin DA. Localised nonlinear modes in the $\mathcal{PT}$-symmetric double-delta well Gross-Pitaevskii equation. Non-Hermitian Hamilt Quantum Phys 2016;184:123–42.
[42] Cartarius H, Wunner G. Model of a $\mathcal{PT}$-symmetric Bose-Einstein condensate in a δ-function double-well potential. Phys Rev A 2012;86:013612.
[43] Abdullaev FK, Kartashov YV, Konotop VV, Zezyulin DA. Solitons in $\mathcal{PT}$-symmetric nonlinear lattices. Phys Rev A 2011;83:041805.
[44] Qi J-J, Zhao D, Liu W-M. Soliton collisions in spin-orbit coupled spin-1 Bose-Einstein condensates. J Phys A 2023;56:255702.
[45] Bersano TM, Gokhroo V, Khamehchi MA, D'Ambroise J, Frantzeskakis DJ, Engels P, Kevrekidis PG. Three-component soliton states in spinor $F = 1$ Bose-Einstein condensates. Phys Rev Lett 2018;120:063202.
[46] Nistazakis HE, Frantzeskakis DJ, Kevrekidis PG, Malomed BA, Carretero-Gonzalez R. Bright-dark soliton complexes in spinor Bose-Einstein condensates. Phys Rev A 2008;77:033612.

[47] Busch T, Anglin JR. Dark-bright solitons in inhomogeneous Bose-Einstein condensates. Phys Rev Lett 2001;87:010401.
[48] Busch T, Anglin JR. Motion of dark solitons in trapped Bose-Einstein condensates. Phys Rev Lett 2000;84:2298–301.
[49] Yang J. Nonlinear waves in integrable and nonintegrable systems. Philadelphia: SIAM; 2010.
[50] Barashenkov IV, Zezyulin DA, Konotop VV. Jamming anomaly in $\mathcal{PT}$-symmetric systems. New J Phys 2016;18:075015.
[51] Fedichev PO, Kagan Y, Shlyapnikov GV, Walraven J. Influence of nearly resonant light on the scattering length in low-temperature atomic gases. Phys Rev Lett 1996;77:2913–6.
[52] Alexeeva NV, Barashenkov IV, Tsironis GP. Impurity-induced stabilization of solitons in arrays of parametrically driven nonlinear oscillators. Phys Rev Lett 2000;84:3053–6.